Nano Energy 137 (2025) 110808

Contents lists available at ScienceDirect

Nano Energy

journal homepage: www.elsevier.com/locate/nanoen

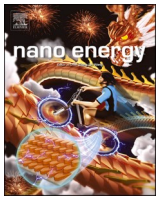

# Fully extended conjugated azo-bridged covalent triazine framework with maximum dual-redox-active sites for advanced lithium organic batteries

Yanxin Yu [a], Qianqian Jin [a], Qiling Li [d], Huapeng Sun [e], Yanbiao Ren [a,*], Shubiao Xia [d,*], Shi Wang [b,c,**], Zhong Jin [c,e,f,***]

[a] College of Chemistry, Chemical Engineering and Materials Science, Zaozhuang University, Zaozhuang 277160, China
[b] State Key Laboratory of Flexible Electronics (LoFE), Institute of Advanced Materials (IAM), School of Chemistry and Life Sciences, Nanjing University of Posts & Telecommunications, 9 Wenyuan Road, Nanjing 210023, China
[c] State Key Laboratory of Coordination Chemistry, MOE Key Laboratory of Mesoscopic Chemistry, MOE Key Laboratory of High Performance Polymer Materials and Technology, Jiangsu Key Laboratory of Advanced Organic Materials, Suzhou Key Laboratory of Green Intelligent Manufacturing of New Energy Materials and Devices, Tianchang New Materials and Energy Technology Research Center, Institute of Green Chemistry and Engineering, School of Chemistry and Chemical Engineering, Nanjing University, Nanjing, Jiangsu 210023, China
[d] College of Chemistry and Environmental Science, Qujing Normal University, Qujing 655011, China
[e] School of New Energy, Chenjiang Laboratory, Chenzhou Vocational Technical College, Chenzhou, Hunan 423000, China
[f] Yoffe Products (Tianchang) Co., Ltd., Tiangchang, Anhui 239300, China

ARTICLE INFO

*Keywords:*
Lithium organic batteries
Organic electrode materials
Covalent triazine frameworks
$Li^+$ storage
Charge conductor

ABSTRACT

Lithium organic batteries based on organic electrode materials (OEMs) have opened up a new way to develop high-performance and environmentally friendly energy storage devices. However, OEMs reported thus far are still severely limited by poor electrical conductivity and unsatisfactory capacity. Herein, we creatively propose to directly conjugate the active motifs with functional linkers in OEMs for simultaneously increasing conductivity and capacity. As the first attempt, an exclusive azo-bridged covalent triazine frameworks (Azo-CTF) where triazine motifs are directly linked with azo groups, is cleverly designed and constructed. By virtue of the thoroughly electron conjugation throughout azo bridges and triazine π units, Azo-CTF with the lowest energy bandgap (2.62 eV) exhibits excellent essential charge conductivity. More excitingly, Azo-CTF achieves maximum redox-active sites integration (with the mass ratio reached to 70 %) to date. Therefore, Azo-CTF anode shows an almost record performance with a high reversible capacity (2332.8 mAh $g^{-1}$ at 0.1 A $g^{-1}$) and inspiring rate characteristics (1034.4 mAh $g^{-1}$ undergoing 500 cycles at 2 A $g^{-1}$, 690.2 mAh $g^{-1}$ undergoing 1000 cycles at 5 A $g^{-1}$). Our work provides a new strategy for synchronously improving the conductivity and capacity of OEMs, which would greatly promote the development of lithium organic batteries.

## 1. Introduction

Lithium-ion batteries (LIBs), as the convenient devices for energy storage, have caused great attention around handy vehicles and smart grids due to the continuous-growing demand of clean energy-storage worldwide. [1–4] The development of effective electrode materials plays an extremely crucial action to promote the performance improvement of LIBs. [5–8] At present, the commercialized inorganic electrode materials not only have the bottleneck of energy density, but also face serious constraints from resource and environment. In contrast, organic electrode materials (OEMs) have attracted extensive attention due to high performance potential, rich structure and sustainability.

* Corresponding authors.
** Corresponding author at: State Key Laboratory of Flexible Electronics (LoFE), Institute of Advanced Materials (IAM), School of Chemistry and Life Sciences, Nanjing University of Posts & Telecommunications, 9 Wenyuan Road, Nanjing 210023, China.
*** Corresponding author at: State Key Laboratory of Coordination Chemistry, MOE Key Laboratory of Mesoscopic Chemistry, MOE Key Laboratory of High Performance Polymer Materials and Technology, Jiangsu Key Laboratory of Advanced Organic Materials, Suzhou Key Laboratory of Green Intelligent Manufacturing of New Energy Materials and Devices, Tianchang New Materials and Energy Technology Research Center, Institute of Green Chemistry and Engineering, School of Chemistry and Chemical Engineering, Nanjing University, Nanjing, Jiangsu 210023, China.
*E-mail addresses:* rybiao1140@163.com (Y. Ren), xiashubiao401@163.com (S. Xia), iamshiwang@njupt.edu.cn (S. Wang), zhongjin@nju.edu.cn (Z. Jin).

https://doi.org/10.1016/j.nanoen.2025.110808
Received 31 May 2024; Received in revised form 11 December 2024; Accepted 20 February 2025
Available online 21 February 2025

Among OEMs, covalent triazine frameworks (CTFs) with robust triazine units have been recognized as a fascinating candidate for LIBs. [9–11] The robust triazine units not only perform as $Li^+$ storage sites to provide potential electrochemical capability, but also confer CTFs with extraordinarily excellent chemical stability and thereby resulting in outstanding cyclic stability. [12–14] In addition, the open and ordered pore channel further increases the exposure of $Li^+$ storage sites and enhances ions diffusion. [15] Therefore, diverse types of CTFs-based electrode materials have been fabricated.[16–19] Unfortunately, CTFs reported so far are failing in terms of their capacity due to either finite active sites or poor conductivity [20].

There are lots of strategies have been reported to adjust the skeleton and craft the functions of CTFs, such as exfoliation, [21,22] composite approach, [23,24] and dual redox-active sites function, [25] however their effects are only in partial. For instance, the exposure of active sites and interfacial area can obtain ascension through exfoliation, but the actual percentage of active sites is unchanged. More poorly, the charge-storage-transport still suffers from enormous loss based on this Van der Waals connections. [26] Composite approach can achieve the enhancement of electrochemical behavior of CTFs-containing electrodes, however, its generality still suffers from rigorous preparation steps, inaccurate active compose, and redundant conductive content. [27] The function of dual redox-active sites endows CTFs-based electrodes with multiple $Li^+$ storage behavior, unfortunately, there are still large inert conjugation skeletons which is only responsible for charge conduction. [25] In other words, the contribution of dual redox-active sites function to date is mainly focused on the improvement of conductivity, which is still failing in maximizing active sites integration, and thereby resulting in unsatisfactory performance. [28–30] Therefore, designing CTFs-based electrodes that meet both excellent conductivity and maximum $Li^+$ storage sites will achieve unsurpassed performance.

Based on the understanding of CTFs mentioned above, herein, we propose to directly conjugate triazine units with other active linkers without additional inactive conjugation skeletons in CTFs for achieving both excellent conductivity and maximum active sites toward satisfying capacity. As the first attempt, a distinctive azo-bridged CTF (Azo-CTF) in which two triazine motifs are straightly linked with azo linkages, is artfully designed and successfully fabricated (Scheme 1). In our design, azo bridges not only meet the basic need as π conjugation system to modulate the electron character of triazine rings, and but also perform as $Li^+$ storage sites, granting Azo-CTF with enough active cores. As assumed and desired, the direct connection between azo linkages and triazine units creates thoroughly electron conjugation throughout the whole structure, and thereby resulting in Azo-CTF with the lowest energy bandgap (2.62 eV) exhibiting strengthened essential charge conductivity via density functional theory (DFT) calculations. More inspiringly, Azo-CTF achieves maximum redox-active sites loading (with the mass percentage reached to 70 % based on the amount of N element in the structure) to date. Benefiting from these merits, Azo-CTF anode displays an unheard capability with a high reversible capacity (2332.8 mAh $g^{-1}$ at 0.1 A $g^{-1}$) and inspiring rate characteristics (1034.4 mAh $g^{-1}$ undergoing 500 cycles at 2 A $g^{-1}$ and 690.2 mAh $g^{-1}$ undergoing 1000 cycles at 5 A $g^{-1}$), which represents one best level compared to previously reported CTFs electrodes and other similar organic electrodes. Our work not only renders the attractive foreground of Azo-CTF anode for LIBs, but also demonstrates an effective strategy to develop desirable CTFs-based electrodes.

## 2. Results and discussion

### 2.1. Azo-CTF preparation and characterizations

As can be seen from Fig. 1a, the fabrication of Azo-CTF is achieved by the self-coupling from melamine using cupper bromide (CuBr) as catalyst in a solvothermal system. All the exhaustive details are described in the Supporting Information. In our design, the construction of azo bridges between two triazine units offers a π electron system, which can not only modulate the electron feature of triazine units, but also facilitate the extended conjugation along the whole skeleton of Azo-CTF, which is responsible for excellent charge conductivity. More attractively, this design simultaneously creates maximum integration of redox-active sites in Azo-CTF with a mass percentage reached to 70 %, which contributes to encouraging performance. Predictably, integrating these virtues into Azo-CTF would achieve unprecedented performance, this upcoming striking outcome encourages us to continue explore its actual performance.

Firstly, the crystal configuration of Azo-CTF was proved through powder X-ray diffraction (PXRD) technology and structure simulation.

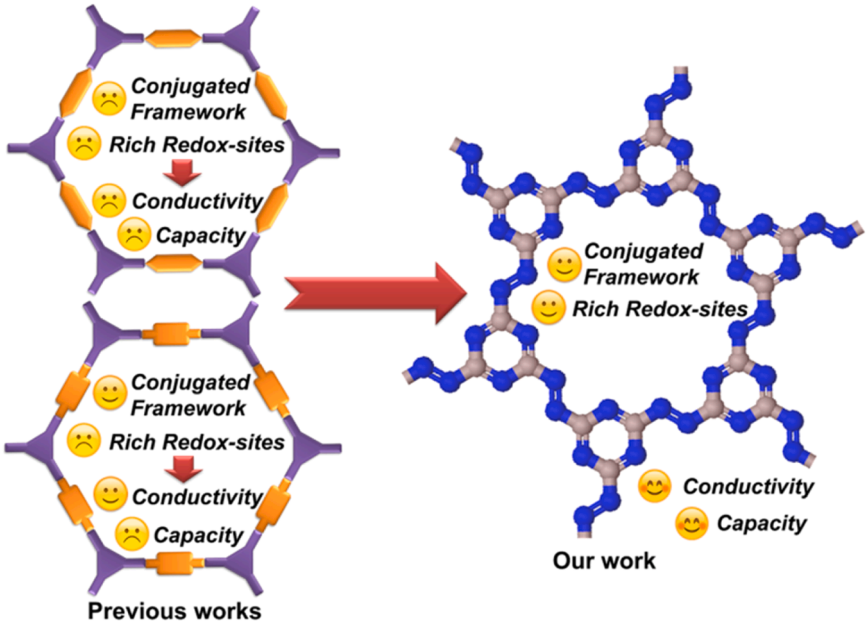


**Scheme 1.** The design of Azo-CTF through the directly conjugated connection between triazine units and azo groups for enhanced natural charge conductivity and maximum redox-active sites loading.

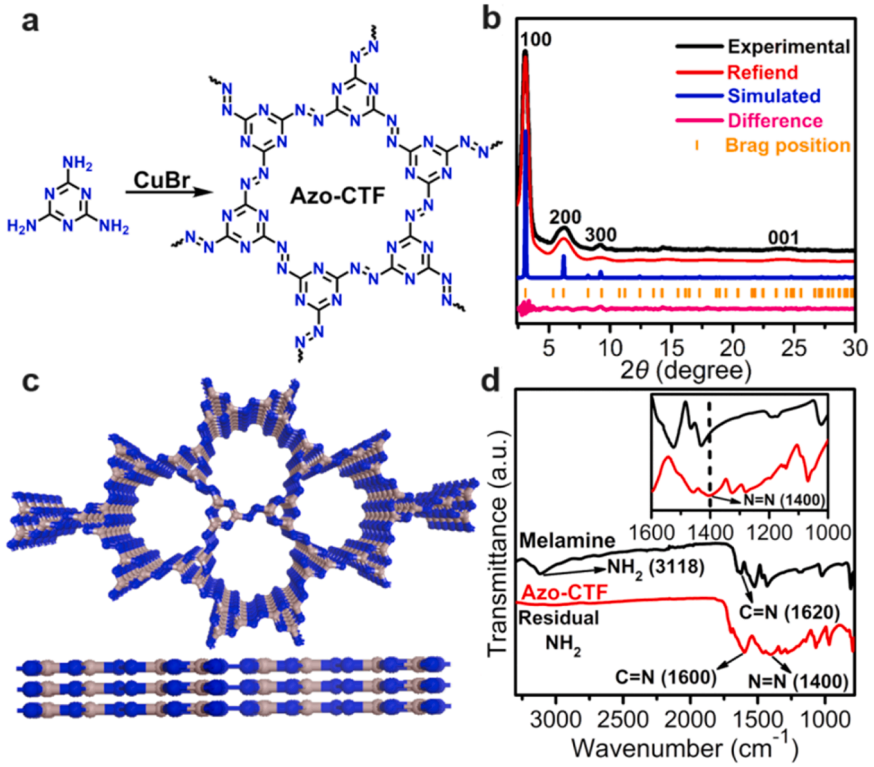


**Fig. 1.** (a) The preparation of Azo-CTF. (b) Experimental PXRD curve and Pawley refinement from the simulated AA stacking model of Azo-CTF. (c) The top and side views on the simulated AA stacking model of Azo-CTF. (d) FT-IR spectra of melamine and Azo-CTF (Inset: The corresponding magnified picture in the wave number range from 1000 to 1600 $cm^{-1}$).

As can be seen from the black curve in Fig. 1b, its experimental PXRD curve exhibits the strongest diffraction at 3.06°, strongly supporting the highly ordered framework of Azo-CTF. In addition, there are three peaks in comparatively feeble intensity at 6.19°, 9.15° and 24.07°, which were determined as belonging to (100), (200), (300) and (001) planes, respectively. The perfect configuration of Azo-CTF was realized from the density functional tight-bingding ($DFTB^+$) calculations. The hexagonal unit cell of Azo-CTF was confirmed in *P6* group space with a = b = 32.94 Å, and c = 3.06 Å, α = β = 90°, γ = 120° through simulated pawley refinement (Fig. 1b, red hollow balls), which further evidenced its experimental PXRD profile. Furthermore, the AA-stacking model of Azo-CTF can satisfactorily match with its experimental PXRD patterns (the blue curve in Figs. 1b, and1c and S1). Comparatively, the PXRD of its staggered AB-stacking structure showed a considerable difference toward the experimental PXRD result (Figure S2). Subsequently, the porosity characteristics of Azo-CTF was certificated via nitrogen adsorption-desorption analysis. As a result, the mesoporous nature of Azo-CTF has been proved from a type II isothermal with a special Brunauer-Emmett-Teller surface area as 350.05 $m^2 g^{-1}$ (Figure S3) and a small as well as incisive pore width of ~3.1 nm (Figure S4), which accorded with the calculated value of 3.0 nm based on its AA-stacking model. Such porosity nature can facilitate the handy transformation of electrolyte composition during charging/discharging process in LIBs, especially $Li^+$. The successful construction of azo bridges in Azo-CTF achieved proof via Fourier transform infrared (FT-IR) analysis (Fig. 1d). For melamine, we can find that the vibration peaks of -$NH_2$ groups and C═N bands in triazine was separately located at 3118 $cm^{-1}$ and 1620 $cm^{-1}$. In contrast, the characteristic peak of -$NH_2$ groups in Azo-CTF was reduced seriously with the remarkable emergence of the vibration band belonged to N = N groups at 1400 $cm^{-1}$. In addition, the peak position of C═N bands has shifted to 1600 $cm^{-1}$ from 1620 $cm^{-1}$ because of the complete conjugation throughout azo bridges and the aromatic triazine-π system in the whole framework of Azo-CTF. Furthermore, the thermal stability of Azo-CTF was assessed through thermogravimetric (TGA) testing. As a result, Azo-CTF can remain stable even at the temperature up to 300 ℃ (Figure S5), showing its sturdy skeleton benefiting from the robust triazine motifs. Finally, its structure was finely appraised via scanning electron microscope (SEM) images (Figure S6). Apparently, the SEM images suggest that Azo-CTF possesses a layered topography, uncovering its excellent 2D network property.

### 2.2. $Li^+$ storage performance of Azo-CTF

After achieving accurate formation of Azo-CTF, its electrochemical behavior was investigated under the voltage window of 0.01–3.0 V in the CR2032-type coin cells. In order to eliminate the interference from some side reactions and solid electrochemical interphase (SEI) on the presentation of redox peaks, [31–33] the cyclic voltammetry (CV) testing was first carried out under the scan rate of 0.1 mV $s^{-1}$ for first cycle and then implemented under the scan rate of 0.2 mV $s^{-1}$ to clear its lithiation/delithiation behavior. As shown in Figure S7, we can easily find notable SEI formation and some side reaction on its CV curve at the scan rate as 0.1 mV $s^{-1}$. More disappointingly, such CV was failed in appearing redox properties of Azo-CTF. Fortunately, the excellent redox behavior of Azo-CTF have been proved by the its CV curve at the scan rate of 0.2 mV $s^{-1}$ (Figure S8). Specifically, there are two significant cathodic peak/anodic peak couples at 1.47/1.13 and 0.61/2.09 V belonged to the reversible lithiumization/delithiumization behavior on triazine units and azo bridges. This result showed the multi-step redox behaviors in Azo-CTF. It is worth mentioning that the CV curves are almost overlapped thoroughly of the initial three cycles, confirming the excellent reversibility and robust $Li^+$ storage behavior of Azo-CTF. This merit has been also proved through the discharge/charge testing. In its first cycle at 0.1 A $g^{-1}$, Azo-CTF anode displays irreversible discharge/charge capacities as 4724.3/1802.5 mAh $g^{-1}$ with the coulombic efficiency (CE) only as 38.2 % (Figure S9). This phenomenon

is primarily resulted from the formation of SEI and the "dead lithium" in the structure of Azo-CTF in the state of the complete discharge, which also often appeared among the non-graphite electrodes. [32] The problem could obtain improvement through pre-lithiation strategy for further practical application. Meanwhile, there are two wide and stable discharging plateau that started from 1.47 V and 0.61 V can be observed, which strongly agrees with the CV curves. The similar match was also appeared between the charging profile and CV curves. In its next two cycles, the discharge/charge performance of Azo-CTF exhibits as 2298.6/1986.0 and 2332.8/2083.7 mAh $g^{-1}$, respectively, indicating this highly reversible $Li^+$ doping/dedoping behavior achieved from its CV curves.

Its rate capability was further explored at the range of current density from 0.1 A $g^{-1}$ to 5 A $g^{-1}$ (Fig. 2a and b). It should be pointed out that some fluctuations of the CE appears during the initial cycles, which could be belonged to the unstable state of Azo-CTF. Meanwhile, there are also some fluctuations in the following cycles due to the voltage drops between two different current densities. Pleasantly, there is no relaxation phenomenon with the addition of current density during all the discharge/charge cycles. More excitingly, Azo-CTF exhibits a desirable capacity as 405.3 mAh $g^{-1}$ at 5 A $g^{-1}$. Particularly, the specific capacity of Azo-CTF still exhibits comparable level toward its started value while backed to 0.1 A $g^{-1}$ again. Inspiringly, such exceptional $Li^+$ storage capability surpassed all previous records of CTFs-based electrodes, such as ACT, [33] Tp-Ta-COF, [34] and so on. In terms of its intrinsic properties, Azo-CTF integrates both excellent electronic conductivity and maximum active loading without large inactive conjugation skeletons, while there are lots of inert contents in other CTFs-based electrodes. Based on this virtue, the $Li^+$ storage performance of Azo-CTF also surpassed other similar organic electrodes relied on network chemistry, for example representative covalent organic frameworks (Figure S10 and Table S1). It could be said that the performance of our Azo-CTF renders one of the record value among OEMs to date. Such result is attributed to the dual efficacy from the fully extended conjugation framework and maximum redox-active sites with a mass percentage of 70 % in Azo-CTF so far. The former is responsible for excellent charge conduction, while the latter provides record $Li^+$ storage sites. Furthermore, Azo-CTF anode performs outstanding cyclability under both 2 A $g^{-1}$ and 5 A $g^{-1}$. It displays a high reversible capacity as 1034.4 mAh $g^{-1}$ at 2 A $g^{-1}$ with the CE closed to 100 % even through 500 cycles (Figure S11). More encouragingly, Azo-CTF still retains an attractive reversible capacity up to 690.2 mAh $g^{-1}$ with the CE reached to 99.8 % at 5 A $g^{-1}$ even undergo 1000 cycles, further emphasizing its high reversibility (Fig. 2c). This inspiring cyclic performance originated from its sturdy and ordered framework, which is competent to meet the needs of the repeated lithiumization/delithiumization. Essentially, all these performance are owed to the direct bridging between triazine units and azo linkages, which gives Azo-CTF with such excellent electrochemical behaviors. Subsequently, its interfacial resistance was achieved from the electrochemical impedance spectrum (EIS) analysis. Pleasantly, there is only a tiny increase (160 Ω) of the interfacial resistance after the 1000-cycles at 5 A $g^{-1}$ than the fresh electrode (Figure S12), rendering again the exceptional cyclability of Azo-CTF which could be attributed to the massive integration of triazine- and azo-active units in its fully conjugated skeleton. Furthermore, its potential of ion diffusion was determined via galvanostatic intermittent titration technique (GITT). [35] As a result (Figure S13), the level of $Li^+$ diffusion coefficient of Azo-CTF in the range of $10^{-10.5}$-$10^{-8.5}$ $cm^2$ $S^{-1}$ is calculated. This excellent $Li^+$ diffusion value of Azo-CTF proves its rapid charge transmission, which could be ascribed to the completed conjugation skeleton as well as the spacious and ordered channel framework.

### 2.3. *$Li^+$ capacity matching of Azo-CTF*

To figure such exceptional rate performance of Azo-CTF electrode out thoroughly, its CV profiles were further explored at the scan rate range of 0.2–1.0 mV $s^{-1}$. As can be seen from Fig. 3a, there are continuous fluctuation of the peak currents with the rising of scan rate, representing the simultaneous occurrence of faradaic and non-faradaic reaction during the lithiumization process of Azo-CTF. [36] Typically, the relationship between the scan rate (v) and obtained corresponding peak current (i) can be illustrated through logarithmic form as log i = b

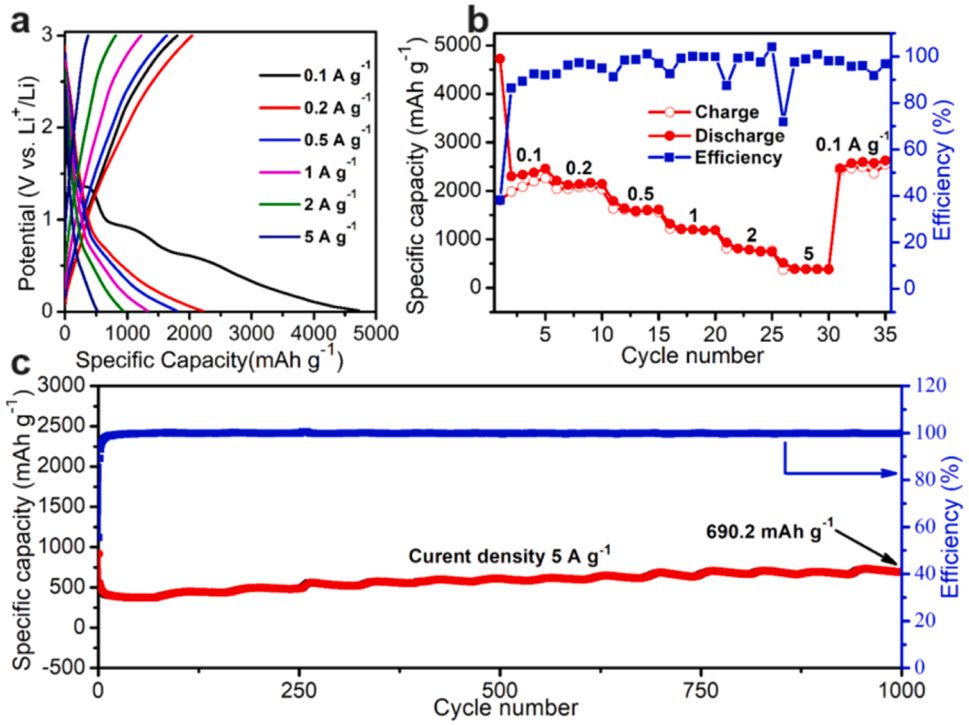


**Fig. 2.** The performance of Azo-CTF anode during discharge/charge process: (a) Discharge/charge curves of the initial cycles at the range of current densities from 0.1 A $g^{-1}$ to 5 A $g^{-1}$. (b) Rate capability at the current density range of 0.1–5 A $g^{-1}$. (c) Long-cycle performance at 5 A $g^{-1}$.

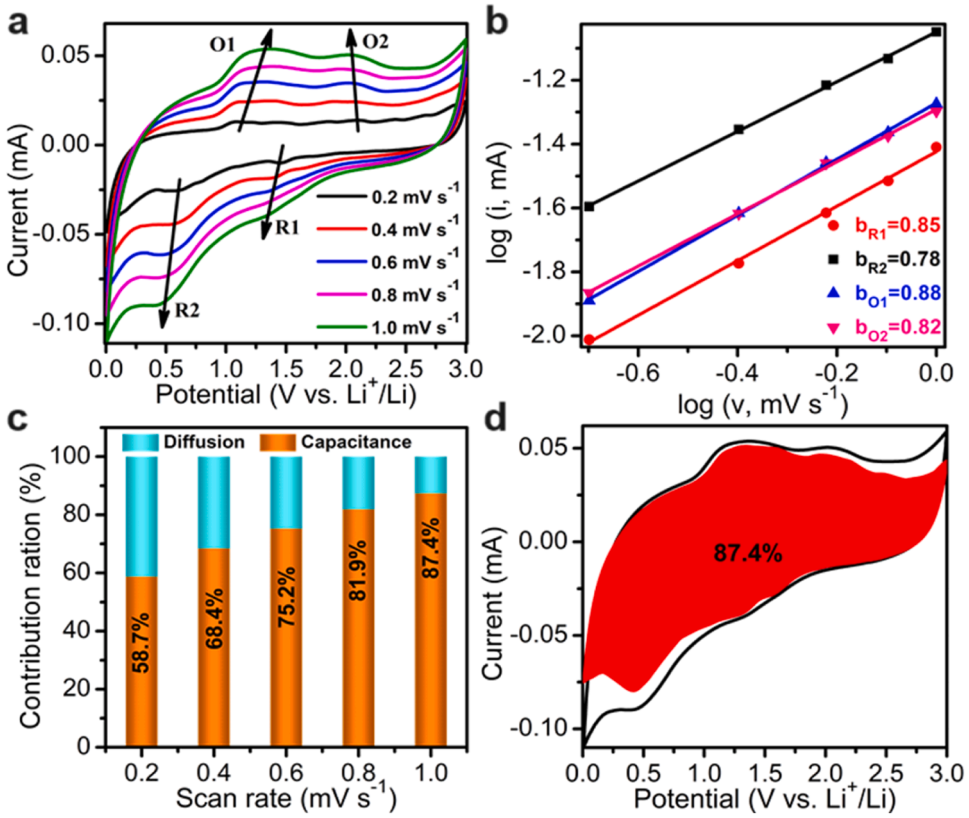


**Fig. 3.** (a) CV curves of Azo-CTF anode at the scan rate ranged from 0.2 mV $s^{-1}$ to 1.0 mV $s^{-1}$. $O_n$ and $R_n$ (n = 1,2) represent the oxidation and reduction peaks, respectively. (b) The b-value of cathodic/anodic peaks. (c) Capacitive-contribution percentage of Azo-CTF anode at the multiple scan rates of 0.2–1.0 mV $s^{-1}$. (d) Contribution percentage of capacitance process at the scan rate of 1.0 mV $s^{-1}$.

log v + log a, in which b = 1 expresses the capacitive-oriented process, and b = 0.5 is on behalf of the diffusion-driveled process. [37,38] The b values for the two cathodic/anodic peak couples of 1.47/1.13 and 0.61/2.09 V are determined as 0.85, 0.88, 0.78 and 0.82 (Fig. 3b), respectively, implying the capacitive-oriented $Li^+$ storage process of Azo-CTF. [39] Such result can be chiefly resulted from the highly reachable redox-active sites as well as the infinite diffusion of $Li^+$ in the porous structure of Azo-CTF. As a result (Fig. 3c, d and Figure S14), The proportion of capacitive contribution has been calculated as 58.7 % at the scan rate of 0.2 mV $s^{-1}$, which rises up to 87.4 % with the increasing of scan rate to 1.0 mV $s^{-1}$. These results reveal the fast capacitive-oriented process for $Li^+$ storage of Azo-CTF-based battery environment, which causes the desirable rate capacity owing to the convenient $Li^+$ transport in the ordered and fully extended conjugation structure of Azo-CTF.

### 2.4. $Li^+$ storage mechanism of Azo-CTF

To best illustrate the lithiumization mechanism of Azo-CTF, ex-situ FT-IR measurement was first recorded to interpret its $Li^+$ storage sites at different discharge/charge points during its first cycle at 0.1 A $g^{-1}$. As shown in Fig. 4b, both vibration peaks of N = N bands at 1400 $cm^{-1}$ of the azo bridges, and C═N bands at 1600 $cm^{-1}$ of the triazine units decreased by degrees during the discharge process, and almost vanished completely when the battery thoroughly discharged. This result suggests that N = N and C═N groups are highly redox-active centers in Azo-CTF. Surprisingly, the peaks of both N = N and C═N bands obtain reappearance with comparable intensity than the fresh Azo-CTF after the recharge to 3.0 V, highlighting the impressive reversibility between the interaction of Azo-CTF and $Li^+$. Moreover, ex-situ X-ray photoelectron spectroscopy (XPS) measurement was implemented for proofing this lithiumization/delithiumization mechanism on N = N and C═N (Fig. 4c). For XPS testing, the initial Azo-CTF was immersed overnight in electrolyte system. In its N 1 s XPS spectrum of the initial Azo-CTF, the curve can be divided into two peaks belong to N = N at 400.20 eV of the azo bridges and N = C-N at 398.55 eV of the triazine units. While fully discharged, these two peaks of N = N and N = C-N both vanished, meanwhile, the signals of N-N (399.91 eV) and N-C-N (398.72 eV) were significantly appeared, supporting the lithiumization of azo and triazine redox-active sites. As anticipated, the signals of N = N and N = C-N get reappearance after the recharge to 3.0 V, supporting the highly reversible lithiumization/delithiumization on azo and triazine sites. This result is in line toward that achieved from the FT-IR analysis, and therefore, the interaction mechanism between $Li^+$ and Azo-CTF can be expressed as presented in Fig. 4d.

For achieving the best understanding between the structure of Azo-CTF and its such exceptional $Li^+$ storage performance, the density functional theory (DFT) calculation was used to illustrate its electron property, which is the determinant for its electrochemcial performance. The electron band of Azo-CTF as well as its density of state (DOS) was also investigated. Meanwhile, the valence and conduction band minimum (VBM and CBM) of Azo-CTF were employed to appraise its ability of charge mobility. In its VBM (Fig. 5a), the electron density shows almost consistent distribution throughout whole the extended conjugation structure, proving the depth reduplication between azo nitrogens and the triazine-π cores. In contrast, the large portion of electron charge centralizes on the region on the azo bridges and only a slightest disperses at the nitrogens of triazine units in the CBM of Azo-CTF (Fig. 5b). Such significant difference of electron density distribution persuasively demonstrates that charge can be caught effectively by triazine traps and further achieves excellent conduction. This result also gets confirmed from its DOS motifs (Fig. 5c). In addition, the energy gap ($E_g$) level of Azo-CTF was calculated as 2.62 eV (Fig. 5d), which further declared the superior inherent electron conductivity and redox ability of Azo-CTF

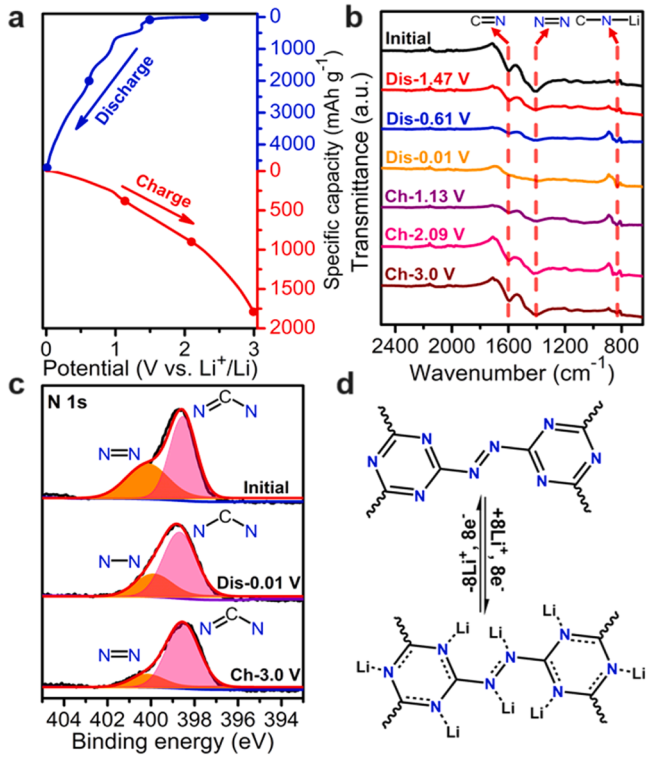


**Fig. 4.** (a) Discharge/charge curves of the first cycle at 0.1 A $g^{-1}$ in the voltage range of 0.01–3.0 V. (b) Ex-situ FT-IR spectrum of Azo-CTF electrode at different lithiumization/delithiumization states. (c) Ex-situ N 1 s XPS spectrum of Azo-CTF electrode at different states. (d) The proposed lithiumization/delithiumization mechanism of Azo-CTF.

benefiting from the fully extend conjugation throughout azo bridges and triazine units. Such extraordinary electron property combined with maximum integration of redox-active sites in the porous and ordered structure of Azo-CTF creates convenient charge transfer and multiple $Li^+$ storage behavior, and thereby achieving its almost record performance in LIBs.

The lithiumization/delithiumization process of Azo-CTF was further explored through DFT calculation to best understand its $Li^+$ storage mechanism. [40] The total energy is performed to appraise the lithiumization sequence and determined as $-6.34 \times 10^4$ eV for Azo-CTF, $-6.71 \times 10^4$ eV for Azo-CTF+ 18Li, and $-6.96 \times 10^4$ eV for Azo-CTF+ 30Li (Fig. 5e). Apparently, there is a difference calculated as $-0.37 \times 10^4$ eV for the total energy of Azo-CTF and Azo-CTF+ 18Li, which proves the lithiumization of the active triazine motifs with 18 Li atoms in Azo-CTF. Using a similar comparison, the difference of the total energy Azo-CTF+ 18Li and Azo-CTF+ 30Li is determined as $-0.25 \times 10^4$ eV, which originated from the sequential lithiumization of N = N bridges with 12 Li atoms in Azo-CTF+ 18Li. It should be clarified that the total energy of Azo-CTF+ 18Li is less than Azo-CTF+ 12Li ($-6.59 \times 10^4$ eV), which indicates that the triazine units preferentially interacts with $Li^+$ over azo groups (Figure S15). During the charge process, the ionization energy of Azo-CTF+ 30Li, Azo-CTF+ 12Li and Azo-CTF are determined as 2.72, 4.32, and 7.02 eV, respectively (Fig. 5e). Apparently, Azo-CTF+ 30Li possesses the lowest ionization energy, indicating that it can release 18 $Li^+$ and convert to Azo-CTF+ 12Li, and then Azo-CTF+ 12Li sequentially to put 12 $Li^+$ out for achieving the reproduce of Azo-CTF. The delithium sequence of the charge process is consistent with the lithium sequence of the discharge process, further supporting the triazine units preferentially interact with $Li^+$ over azo groups. Therefore, the sequence of lithiumization/delithiumization of Azo-CTF can be expressed as Fig. 5f. From these results, it can achieve such conclusion as the efficient utilization of the $Li^+$ storage sites integrated by triazine units and azo groups creates a theoretical capacity reached to 1340.3 mAh $g^{-1}$. Such exciting theoretical capability can be benefited from the maximum integration of redox-active sites in Azo-CTF with the mass percentage of 70 %, which is out of that in previously reported CTFs-based electrodes and other types of OEMs. It should be pointed out that the experimental performance of Azo-CTF, especially at low current density is higher than the theoretical capacity, which is a frequently occurred phenomenon also in other reported materials. [41] For electrode materials, their theoretical capacity are related to the amount of the stored $Li^+$. Through CV analysis described above, we can know that there is a multistep $Li^+$ intercalation process of Azo-CTF which is not only interact with C=N and N = N storage sites. Furthermore, the fast capacitive-oriented process caused by the adsorption of $Li^+$ on the surface of Azo-CTF, which also contributed to the desirable capacity. All of these results lead to the experimental performance higher than the theoretical level.

### 2.5. Practical implications and potential applications

The successful development of Azo-CTF with significantly enhanced conductivity and maximum redox-active sites presents profound practical implications for the advancement of lithium organic batteries (LOBs). The unprecedented electrochemical performance of Azo-CTF underscores its potential as a promising electrode material for high-performance energy storage. This would be particularly valuable for portable electronics, electric vehicles, and grid-scale energy storage systems. Meanwhile, the use of Azo-CTF could offer a sustainable alternative based no the considering of the environmental concerns associated with traditional battery technology. The abundance and recyclability of organic electrode make Azo-CTF as a promising candidate for green energy storage solution. Furthermore, the convenient synthesis provides the possibility to integrate Azo-CTF into commercial LOBs. The synthesis of Azo-CTF through a solvothermal self-coupling by melamine is relatively straightforward and scalable. This is expected to facilitate the production of large quantities of azo-functionalized CTFs-based materials for commercial applications. Besides, melamine with the feature of abundant and inexpensive makes Azo-CTF as a cost-effective alternative to traditional inorganic electrode materials. In conclusion, the development of Azo-CTF not only advances the scientific understanding of OEMs, but also presents exciting opportunities for practical applications in high-performance, sustainable, and cost-effective energy storage solutions. The feasibility of integrating Azo-CTF into commercial LOBs is promising, and further research and development efforts will undoubtedly pave the way for its widespread adoption.

## 3. Conclusions

Briefly summary, the strategy of the function integration of triazine units and azo groups in Azo-CTF through directly conjugated connection without additional inert conjugation skeleton for desirable $Li^+$ storage performance have been rendered. In Azo-CTF, azo linkages as the conjugated-π electron system can not only adjust the electron property of triazine units, but also act as the excellent redox-active centers, endowing Azo-CTF with rich $Li^+$ storage sites and excellent charge conduction. Attributing to the thoroughly electron conjugation throughout azo nitrogens and triazine π system, Azo-CTF with the lowest $E_g$ calculated as 2.62 eV demonstrates improved natural charge conductivity via DFT calculations. More inspiringly, the directly conjugated integration of triazine units and azo groups creates Azo-CTF achieving maximum redox-active sites loading (with the mass percentage reached to 70 %) to date. By these virtues, Azo-CTF anode achieves an almost record performance with a high reversible capacity (2332.8 mAh $g^{-1}$ at 0.1 A $g^{-1}$) and impressive rate characteristics (1034.4 mAh $g^{-1}$ at 2 A $g^{-1}$ undergoing 500 cycles and 690.2 mAh $g^{-1}$ at 5 A $g^{-1}$ undergoing 1000 cycles). The achieved performance of Azo-CTF not only

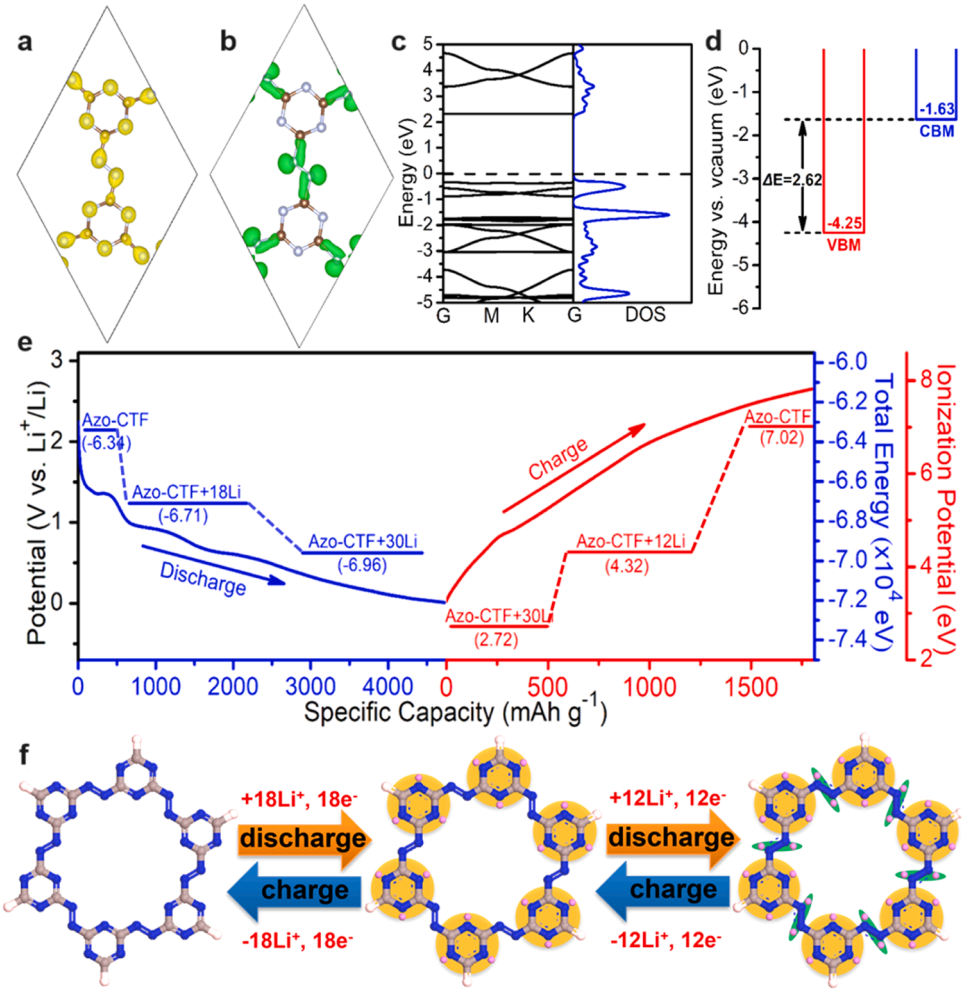


**Fig. 5.** (a) The VBM and (b) CBM electron density of Azo-CTF, the grey and brown balls represent the carbon and nitrogen atoms, respectively. (c) The band structures and DOS of Azo-CTF. (d) The simulated VBM and CBM energy value of Azo-CTF. (e) Proposed lithiumization/delithiumization process of Azo-CHF electrode. (f) Schematic diagram for structural formation of Azo-CTF under different lithiumization/delithiumization states.

represents its attractive potential for $Li^+$ storage, but also opens an new strategy and insight to design and fabricate advanced CTFs-based electrodes.

## CRediT authorship contribution statement

**Xia Shubiao:** Visualization, Funding acquisition, Conceptualization. **Sun Huapeng:** Software, Resources, Conceptualization. **Ren Yanbiao:** Visualization, Validation, Conceptualization. **Jin Qianqian:** Methodology, Formal analysis, Data curation. **Li Qiling:** Validation, Data curation. **Yu Yanxin:** Writing – review & editing, Writing – original draft, Conceptualization. **Wang Shi:** Writing – review & editing, Funding acquisition. **Jin Zhong:** Validation, Funding acquisition, Conceptualization.

## Declaration of Competing Interest

All authors declare no competing financial interest.

## Acknowledgments

We acknowledge financial support from the National Natural Science Foundation of China (22169016, 22479074, 22475096), the Natural Science Foundation of Jiangsu Province (BK20210601, BK20240400, BK20241236), the China Postdoctoral Science Foundation (2023M741624), the Project of State Key Laboratory of Organic Electronics and Information Displays, NJUTP (GZR2023010016), the Natural Science Foundation of NJUTP (NY223079), the Natural Science Foundation of Shandong Province (ZR2023QB090, ZR2021MB100), the General Project of the Joint Fund of Equipment Pre-research and the Ministry of Education (8091B02052407), the Natural Science Foundation of Jiangsu Province (BK20240400 and BK20241236), the Science and Technology Major Project of Jiangsu Province (BG2024013), the Scientific and Technological Achievements Transformation Special Fund of Jiangsu Province (BA2023037), the Key Core Technology Open Competition Project of Suzhou City (SYG2024122), the Gusu Leading Talent Program of Scientific and Technological Innovation and Entrepreneurship of Wujiang District in Suzhou City (ZXL2021273), and the Chenzhou National Sustainable Development Agenda Innovation Demonstration Zone Provincial Special Project (2023sfq11). China Postdoctoral Science Foundation (2023M741624), the Project of State Key Laboratory of Organic Electronics and Information Displays, Nanjing University of Posts and Telecommunications (NJUTP) (No. GZR2023010016), Natural Science Foundation of NJUTP (Grant Nos. NY223079 and NY224199). Natural Science Foundation of Jiangsu Province (BK20210601).

*Author contributions*

The original idea was conceived by Y.-X.Y., Z.J., S.W., S.-B.X., and Y.-

B.R.; Experiments and data analyses were performed by Y.-X.Y., Q.-Q.J., Q.-L.L., and H.-P. S.; Structure characterizations were performed by Y.-X.Y.; and the manuscript was drafted by Y.-X.Y., Z.J., S.W., S.-B.X., and Y.-B.R.

*Supporting information*

Supporting information can be found online.

## Appendix A. Supporting information

Supplementary data associated with this article can be found in the online version at doi:10.1016/j.nanoen.2025.110808.

## Data availability

Data will be made available on request.

## References


[1] S. Ma, J. Zhao, Q. Gao, C. Song, H. Xiao, F. Li, G. Li, Breaking mass transport limitations by iodized polyacrylonitrile anodes for extremely fast-charging lithium-ion batteries, Angew. Chem. Int. Ed. 62 (2023) e202315564.

[2] Q. Sun, Z. Cao, Z. Ma, J. Zhang, W. Wahyudi, G. Liu, H. Cheng, T. Cai, E. Xie, L. Cavallo, Q. Li, J. Ming, Interfacial and interphasial chemistry of electrolyte components to invoke high-performance antimony anodes and non-flammable lithium-ion batteries, Adv. Funct. Mater. 33 (2023) 2210292.

[3] X. Fan, C. Wang, High-voltage liquid electrolytes for Li batteries: progress and perspectives, Chem. Soc. Rev. 50 (2021) 10486–10566.

[4] S. Liu, F. Peng, Y. Lin, W. Zhou, W. Huang, Structural modification enhances the electrochemical performance for organic cathode material, Chem. Eng. J. 451 (2023) 139076.

[5] X. Xu, S. Zhang, K. Xu, H. Chen, X. Fan, N. Huang, Janus dione-based conjugated covalent organic frameworks with high conductivity as superior cathode materials, J. Am. Chem. Soc. 145 (2023) 1022–1030.

[6] L. Zhou, J. Zhang, Y. Wu, W. Wang, H. Ming, Q. Sun, L. Wang, J. Ming, H. Alshareef, Understanding ostwald ripening and surface charging effects in solvothermally-prepared metal oxide-carbon anodes for high performance rechargeable batteries, Adv. Energy Mater. 9 (2019) 1902194.

[7] L. Chen, L. Cheng, J. Yu, H. Wang, F. Cui, G. Zhu, Tailored organic cathode material with multi-active site and compatible groups for stable quasi-solid-state lithium-organic batteries, Adv. Funct. Mater. 32 (2022) 2209848.

[8] Q. Sun, Z. Cao, Z. Ma, J. Zhang, H. Cheng, X. Guo, G. Park, Q. Li, E. Xie, L. Cavallo, Y. Sun, J. Ming, Dipole-dipole interaction induced electrolyte interfacial model to stabilize antimony anode for high-safety lithium-ion batteries, ACS Energy Lett. 10 (2022) 3545–3556.

[9] G. Zhao, H. Li, Z. Gao, L. Xu, Z. Mei, S. Cai, T. Liu, X. Yang, H. Guo, X. Sun, Dual-active-center of polyimide and triazine modified atomic-layer covalent organic frameworks for high-performance Li storage, Adv. Funct. Mater. 31 (2021) 2101019.

[10] C. Wu, M. Hu, X. Yan, G. Shan, J. Liu, J. Yang, Azo-linked covalent triazine-based framework as organic cathodes for ultrastable capacitor-type lithium-ion batteries, Energy Storage Mater. 36 (2021) 347–354.

[11] K. Sakaushi, G. Nickerl, F.M. Wisser, D.N. Hamane, E. Hosono, H. Zhou, S. Kaskel, J. Eckert, An energy storage principle using bipolar porous polymeric frameworks, Angew. Chem. Int. Ed. 51 (2012) 7850.

[12] C. Krishnaraj, H.S. Jena, K. Leus, P. Van Der Voort, Covalent triazine frameworks–a sustainable perspective, Green. Chem. 22 (2020) 1038–1071.

[13] M. Liu, L. Guo, S. Jin, B. Tan, Covalent triazine frameworks: synthesis and applications, J. Mater. Chem. A. 7 (2019) 5153–5172.

[14] Y. Zhang, S. Jin, Recent advancements in the synthesis of covalent triazine frameworks for energy and environmental applications, Poly. Bull. 11 (2019) 31.

[15] T. Sun, C. Wang, Y. Xu, Covalent triazine framework nanosheets for efficient energy storage and conversion, Chem. Res. Chin. Univ. 36 (2020) 640–647.

[16] Y. Su, Y. Liu, P. Liu, D. Wu, X. Zhang, F. Zhang, X. Feng, Compact coupled graphene and porous polyaryltriazine-derived frameworks as high performance cathodes for lithium-ion batteries, Angew. Chem. Int. Ed. 54 (2015) 1812.

[17] O. Buyukcakir, J. Ryu, S.H. Joo, J. Kang, R. Yuksel, J. Lee, S. Choi, S. Lee, S. Kwak, S. Park, R. Ruoff, Lithium accommodation in a redox-active covalent triazine framework for high areal capacity and fast-charging lithium-ion batteries, Adv. Funct. Mater. 1 (2020) 30.

[18] K.A. See, S. Hug, K. Schwinghammer, M.A. Lumley, Y. Zheng, J. Nolt, G. Stucky, F. Wudl, B. Lotsh, R. Seshadri, Lithium charge storage mechanisms of cross-linked triazine networks and their porous carbon derivatives, Chem. Mater. 27 (2015) 3821–3829.

[19] Z. Wang, S. Gu, L. Cao, L. Kong, Z. Wang, N. Qin, M. Li, W. Luo, J. Chen, S. Liu, H. Yuan, Y. Bai, K. Zhang, Z. Lu, Redox of dual-radical intermediates in a methylene-linked covalent triazine framework for high-performance lithium-ion batteries, ACS Appl. Mater. Interfaces 13 (2021) 514–521.

[20] L. Zhou, J. Seonyong, P. Mihui, F. Liang, K. Zhang, Y. Fan, Z. Hao, Structural engineering of covalent organic frameworks for rechargeable batteries, Adv. Energy Mater. 11 (2021) 2003054.

[21] H. Zhang, W. Sun, X. Chen, Y. Wang, Few-layered fluorinated triazine-based covalent organic nanosheets for high performance alkali organic batteries, ACS Nano 13 (2019) (2019) 14252–14261.

[22] Y. Zhu, X. Chen, Y. Cao, W. Peng, Y. Li, G. Liang, F. Zhang, X. Fan, Reversible intercalation and exfoliation of layered covalent triazine frameworks for enhanced lithium ion storage, Chem. Commun. 55 (2019) 1434–1437.

[23] Z. Lei, X. Chen, W. Sun, Y. Zhang, Y. Wang, Exfoliated triazine-based covalent organic nanosheets with multielectron redox for high-performance lithium organic batteries, Adv. Energy Mater. 9 (2019) 1801010.

[24] K. Li, Y. Wang, B. Gao, X. Lv, Z. Si, H. Wang, Conjugated microporous polyarylimides immobilization on carbon nanotubes with improved utilization of carbonyls as cathode materials for lithium/sodium-ion batteries, J. Coll. Inter. Sci. 601 (2021) 446–453.

[25] G. Zhao, Y. Sun, Y. Yang, C. Zhang, Q. An, H. Guo, Molecular engineering regulation redox-dual-active-center covalent organic frameworks-based anode for high-performance Li storage, EcoMat 4 (2022) e12221.

[26] J. Liang, Y. Zheng, J. Chen, J. Liu, D. Hulicova-Jurcakova, M. Jaroniec, S. Qiao, Facile oxygen reduction on a three-dimensionally ordered macroporous graphitic $C_3N_4$/carbon composite electrocatalyst, Angew. Chem. Int. Ed. 51 (2012) 3892.

[27] Q. Fan, J. Su, T. Sun, Z. Bi, H. Wang, S. Zhang, Q. Liu, L. Zhang, G. Hu, Advances of the functionalized carbon nitrides for electrocatalysis, Carbon Energy 4 (2022) 211.

[28] G. Zhao, Y. Zhang, Z. Gao, H. Li, S. Liu, S. Cai, X. Yang, H. Guo, X. Sun, Dual active site of the Azo and carbonyl-modified covalent organic framework for high-performance Li storage, ACS Energy Lett. 5 (2020) 1022–1031.

[29] X. Yang, L. Gong, X. Liu, P. Zhang, B. Li, D. Qi, K. Wang, P. He, J. Jiang, Mesoporous polyimide-linked covalent organic framework with multiple redox-active sites for high-performance cathodic Li storage, Angew. Chem. Int. Ed. 61 (2022) e202207043.

[30] Y. Cao, W. Sun, C. Guo, L. Zheng, M. Yao, Y. Wang, Rational construction of yolk–shell bimetal-modified quinonyl-rich covalent organic polymers with ultralong lithium-storage mechanism, ACS Nano 16 (2022) 9830–9842.

[31] S. Xia, Y. Cai, L. Yao, J. Shi, F. Cheng, J. Liu, Z. He, J. Zheng, Nitrogen-rich two-dimensional π-conjugated porous covalent quinazoline polymer for lithium storage, Energy Storage Mater. 50 (2022) 225–233.

[32] J. Yan, Y. Cui, M. Xie, G. Yang, D. Bin, D. Li, Immobilizing redox-active tricycloquinazoline into a 2D conductive metal–organic framework for lithium storage, Angew. Chem. Int. Ed. 60 (2021) 24467.

[33] Y. Tong, J. Wang, Z. Sun, W. Huang, Extremely-long-lifedspan and ultrahigh-rate Li-ion batteries using conjugated porous triazine polymers, ACS Appl. Mater. Interfaces 15 (2023) 14274–14281.

[34] G. Zhao, Y. Sun, Y. Yang, C. Zhang, Q. An, H. Guo, Molecular engineering regulation redox-dual-active-center covalent organic frameworks-based anode for high-performance Li storage, EcoMat 4 (2022) (2022) e12221.

[35] M. Zhang, Y. Tong, Z. Sun, J. Wang, Y. Lin, F. Kang, Q. Zhang, W. Huang, Two-dimensional covalent organic framework with synergistic active centers for efficient electrochemical sodium storage, Chem. Mater. 35 (2023) 4873–4881.

[36] S.-Y. Li, W.-H. Li, X.-L. Wu, Y. Tian, J. Yue, G. Zhu, Pore-size dominated electrochemical properties of covalent triazine frameworks as anode materials for K-ion batteries, Chem. Sci. 10 (2019) 7695–7701.

[37] J. Wang, J. Polleux, J. Lim, B. Dunn, Pseudocapacitive contributions to electrochemical energy storage in $TiO_2$ (anatase) nanoparticles, J. Phys. Chem. C. 111 (2007) 14925.

[38] V. Augustyn, P. Simon, B. Dunn, Pseudocapacitive oxide materials for high-rate electrochemical energy storage, Energy Environ. Sci. 7 (2014) 1597–1614.

[39] H. Banda, J.-H. Dou, T. Chen, N.J. Libretto, M. Chaudhary, G. Bernard, J. Miller, V. Michaelis, M. Dincă, High-capacitance pseudocapacitors from $Li^+$ ion intercalation in nonporous, electrically conductive 2D coordination polymers, J. Am. Chem. Soc. 143 (2021) 2285.

[40] C. Peng, G. Ning, J. Su, G. Zhong, W. Tang, B. Tian, C. Su, D. Yu, L. Zu, J. Yang, M. Ng, Y. Hu, Y. Yang, M. Armand, K. Loh, Reversible multi-electron redox chemistry of π-conjugated N-containing heteroaromatic molecule-based organic cathodes, Nat. Energy 2 (2021) 17074.

[41] J. Yin, N. Li, M. Liu, Z. Li, X. Wang, M. Chen, M. Zhong, W. Li, Y. Xu, X. Bu, Stabilizing redox-active hexaazatriphenylene in a 2D conductive metal–organic framework for improved lithium storage performance, Adv. Funct. Mater. 33 (2023) 2211950.